Optics Letters

# Patterned multilayer metamaterial for fast and efficient photon collection from dipolar emitters

O. A. Makarova, M. Y. Shalaginov, S. Bogdanov, A. V. Kildishev, A. Boltasseva, and V. M. Shalaev*

*School of Electrical & Computer Engineering, Birck Nanotechnology Center, and Purdue Quantum Center, Purdue University, West Lafayette, Indiana 47907, USA*
**Corresponding author: shalaev@purdue.edu*

*Received 8 August 2017; revised 31 August 2017; accepted 2 September 2017; posted 8 September 2017 (Doc. ID 303875); published 27 September 2017*

**Solid-state quantum emitters are prime candidates for the realization of fast, on-demand single-photon sources. The improvement in photon emission rate and collection efficiency for point-like emitters can be achieved by using a near-field coupling to nanophotonic structures. Plasmonic metamaterials with hyperbolic dispersion have previously been demonstrated to significantly increase the fluorescence decay rates from dipolar emitters due to a large broadband density of plasmonic modes supported by such metamaterials. However, the emission coupled to the plasmonic modes must then be outcoupled into the far field before it succumbs to ohmic losses. We propose a nano-grooved hyperbolic metamaterial that improves the collection efficiency by several times compared to a conventional planar lamellar hyperbolic metamaterial. Our approach can be utilized to achieve broadband enhancement of emission for diverse types of quantum emitters.** 

***OCIS codes:*** (160.3918) Metamaterials; (310.6628) Subwavelength structures, nanostructures; (250.5230) Photoluminescence.

https://doi.org/10.1364/OL.42.003968

Efficient generation of single photons is important for applications in quantum information, such as quantum computation [1], quantum key distribution [2], and transfer of quantum information [3]. Ideally, such a source must produce only one photon on demand with a high repetition rate and directionality. Integrated single-photon sources (SPS) have been demonstrated based on various emitters, including color centers in diamond [4–8]; quantum dots [9]; and defects in SiC [10], ZnO [11], and two-dimensional (2D) materials [12]. Numerous applications in quantum communications, such as quantum key distribution and the generation of large cluster states, require deterministically controlled SPS. A deterministic SPS can be achieved by efficiently collecting the fluorescence signal from a single-photon emitter. Efficient photon collection is also important for magnetometry [13–15] and biosensing [16] applications where emitter ensembles are utilized. The improvement in photon emission rate and collection efficiency for point-like emitters can be achieved by near-field coupling to nanophotonic/plasmonic structures, such as plasmonic waveguides [17], bullseye gratings [18], as well as photonic crystals [19,20], nanopatch [21], and Yagi-Uda [22] antennas. In the case of emitters with relatively broad emission spectra, dielectric structures such as photonic crystal cavities may not fit well, since they only enhance a relatively narrow part of the emission spectrum. Plasmonic nanoantennas such as patch antennas [23–25] or bullseye gratings [26,27] and other structures (see [28] for a recent comprehensive review) provide broader resonances, suitable for specific room-temperature emitters. The spectral response in these structures, however, is still limited by the resonance condition.

Metamaterials with hyperbolic dispersion, known as hyperbolic metamaterials (HMM) [29–32], were shown to provide very large enhancement of the photonic density of states in a broad wavelength range. The enhanced density of states in HMMs is not caused by a resonance, but instead results from the HMM's highly anisotropic optical behavior. Hence, near-field coupling of SPS to an HMM can lead to a significant broadband enhancement of the emission rate [33–35]. This enhancement occurs as long as the emission spectrally overlaps with the frequency region of the hyperbolic dispersion. HMMs are therefore uniquely suitable for efficient coupling to a variety of emitters. However, previous experimental studies of emitters on planar HMMs [36–40] showed that the power emitted by a dipole emitter (which is released in the form of propagating plasmonic waves inside of the HMM) is eventually dissipated inside the metamaterial due to ohmic losses [41,42]. Patterning of the HMM surface can scatter the HMM plasmonic waves into the far field, significantly improving the photon collection efficiency [27,43–45]. In this work, we propose utilizing a nanostructured HMM to improve the collection efficiency over a broad wavelength range (600–800 nm).

Numerical modeling is performed using a commercial finite element solver (COMSOL Multiphysics, Wave Optics Module). The proposed design is based on a circular groove defined in a planar lamellar HMM grown on a metal substrate (see Fig. 1). We analyze the power collection efficiency dependence on the groove geometrical parameters, dipole orientation, and emission wavelength. The outcoupling structure consists of three regions: a central HMM cylinder ($0 < r < r_c$), a circular

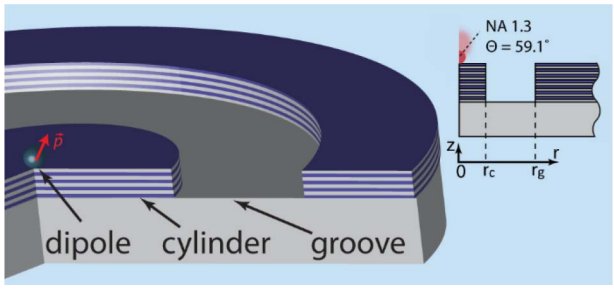


**Fig. 1.** Geometry of the patterned metamaterial structure used for enhancing the emission rate and collection efficiency from dipolar emitters. Collection efficiency is calculated for an oil immersion objective with NA 1.3 (corresponding cross-section angle 59.1°).

groove ($r_c \le r \le r_g$), and an exterior planar HMM region ($r > r_g$) (Fig. 1). Using this structure, we aim at improving the collected photon rate from the emitter compared to the case of a planar, unstructured multilayer HMM. This is achieved by attaining high collection efficiency while keeping a relatively high Purcell factor for both dipole orientations.

The HMM is modeled as a binary superlattice of alternating layers of a crystalline metal (Ag) and dielectric [(Al, Sc)N]. Ag is chosen as the plasmonic material due to its low losses in the visible range and (Al, Sc)N as a crystalline dielectric material, which can be lattice-matched with Ag, resulting in epitaxial films. Epitaxial growth should result in a better control of layer thicknesses and film quality compared to that of an HMM that is composed of polycrystalline/amorphous materials. The figure of merit for the surface plasmon modes for the Ag/(Al, Sc)N HMM is two orders of magnitude higher compared to the epitaxial TiN/(Al, Sc)N HMM [38,46]. The proposed superlattice can be fabricated adopting the DC magnetron sputtering technique described in Ref. [47]. The planar HMM consists of eight binary layers, with elementary layer thicknesses being $t_{\mathrm{met}} = 10$ nm and $t_{\mathrm{diel}} = 20$ nm of Ag and (Al, Sc)N, respectively, resulting in a total thickness of $t_{\mathrm{HMM}} = 240$ nm. The thickness of the layers is chosen to maximize the Purcell factor at a wavelength of 685 nm. The proposed HMM possesses hyperbolic properties over the entire wavelength range of study. The permittivities of Ag and (Al, Sc)N are $\varepsilon_{\mathrm{met}} = -21.84 + 0.396i$ [48] and $\varepsilon_{\mathrm{diel}} = 5.07 + 0.12i$ [38], respectively. In our simulation, the superstrate is immersion oil with a refractive index of 1.515, and the substrate is made of silver.

The dipole emitter is modeled as a current oscillating inside a 2-nm-diameter sphere. To imitate a nitrogen-vacancy (NV) center in a nanodiamond, we have placed the dipole in the center of a dielectric sphere with a refractive index of 2.42 and a radius of 25 nm. The emission wavelength was swept between 585 and 785 nm. The total dissipated power is computed as an integral of power flux through a 6-nm-diameter sphere surrounding the emitter sphere. The ratio of the total dissipated power (Pt) for the emitter in the structure and a dipole in the nanodiamond in a vacuum is defined as the Purcell factor (PF). The collected power (Pc) is calculated as an integral through a circular area above the emitter, which mimics the emission collection using a commercially available objective lens with numerical aperture (NA) 1.3 (cross-section angle 59.1°). The collection efficiency $\beta$ is defined as Pc/Pt. Two different dipole orientations are considered in the study: the radial ($r$, along the $r$ axis) and axial ($z$, along the $z$ axis). The emitter is placed at $r = 0$ and $z = 25$ nm above the HMM surface [Fig. 2(a)].

The parameter space for this structure is large, including the central cylinder radius ($r_c$), groove width ($w_g$), the number of layer pairs, choice of top layer [Ag or (Al, Sc)N], and substrate material (Ag or MgO). Instead of rigorously optimizing the performance over the entire parameter space, we have fixed most parameters using intuitive reasoning. In particular, we chose a cylinder radius $r_c$ that allows the formation of a surface plasmon polariton (SPP) mode on the HMM/oil interface [49]. The surface plasmon possesses a wave vector with $k_r = k_r' + k_r'' = (1.49 \times 10^7 + i3.88 \times 10^4)\ \mathrm{m}^{-1}$, and the choice of $r_c = 100\ \mathrm{nm} > k_r'^{-1}$ is reasonable. At the same time, this cylinder radius is smaller than the SPP propagation length of $k_r''^{-1} = 12.9\ \mu\mathrm{m}$, avoiding plasmonic losses in the cylinder. The top layer is chosen to be dielectric to limit the emitter quenching rate. Ag is proposed as a substrate material to act as a mirror and prevent the propagation of the emission into the substrate. To finalize the design, we optimized the width of the groove $w_g$.

Compared to the case of a planar, unstructured HMM, we observed a significant improvement in $\beta$ over a broad wavelength range for the proposed groove structure. PF was consistently high (from 24 to 39 for the $z$ dipole and $11 \pm 1$ for the $r$ dipole) over the studied wavelength range, promising fast emission dynamics typically observed in plasmonic nanostructures. The parameters of the final structure are presented in Fig. 2(a), and the resulting spectra of $\beta$ for the $z$ and $r$ dipoles are shown in Figs. 2(b) and 2(c), respectively. We note that a nanodiamond radius change from 20 to 40 nm results in relative $\beta$ variations by less than 15%. In the rest of the Letter, we consider the nanodiamond radius to be fixed at 25 nm.

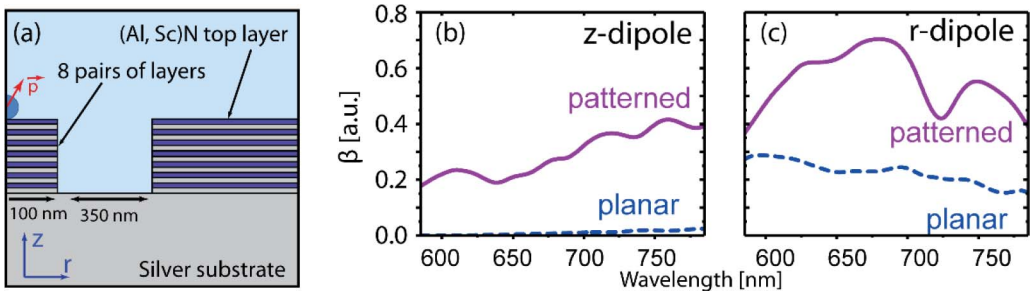


**Fig. 2.** (a) Geometry of the proposed outcoupling structure. The collection efficiency $\beta$ for the (b) $z$- and (c) $r$-oriented dipoles [see (a) for direction] for patterned and planar hyperbolic metamaterial (HMM).

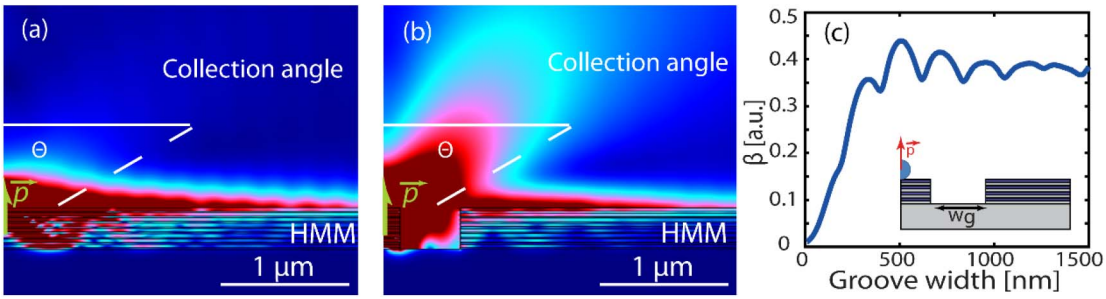


**Fig. 3.** Power density distribution for a $z$-oriented dipole on a (a) planar HMM ($r_c \to \infty$) and (b) patterned HMM. The structure allows outcoupling at the cylinder corner, resulting in the increase of $\beta$ by a factor of 40 for a 685-nm emission wavelength. (c) Dependence of $\beta$ on the groove width $w_g$ for the $z$ dipole at a 685-nm emission wavelength. The objective coupling efficiency saturates for the $z$ dipole as the groove becomes wide enough. The SPP that is scattered at the cylinder corner experiences weaker coupling back to the metamaterial.

However, $\beta$ behaves very differently depending on the dipole orientation.

The $z$ dipole experiences the strongest coupling to metamaterial modes [41,42]. In the case of a planar HMM ($r_c \to \infty$), the coupling results in $\beta < 3\%$ [Fig. 2(b)]. Most of the emitted power eventually gets absorbed in the metamaterial in the form of plasmons without being outcoupled to free space [Fig. 3(a)]. Nano-groove patterning of the HMM helps to increase $\beta$ by at least a factor of 16 across the whole wavelength range compared to the case of a planar HMM. The improvement is mostly attributed to the surface plasmons propagating on the air–HMM interface being scattered into the superstrate by the cylinder corners at $r = r_c$ [Fig. 3(b)].

The groove width ($w_g$) significantly affects the value of $\beta$ [Fig. 3(c)]. For groove widths under 300 nm, the propagating SPP with a wavelength of about 420 nm experiences tunneling through the groove. When the groove width exceeds the size of the SPP wavelength, the tunneling is prevented, and $\beta$ reaches the approximate value of $37 \pm 3\%$. The oscillations about the asymptotic value are caused by partial leaking of surface plasmons into the plasmonic cavity that is formed by the walls of the groove.

For the $r$ dipole, the planar HMM essentially acts as a reflecting mirror. This effect results in $\beta$ of 15%, which is significantly higher compared to the $z$ dipole case. The groove pattern allows increasing $\beta$ for this dipole orientation to at least 35%. To understand this enhancement, we note that the $r$ dipole emission experiences a different environment depending on the $k$ vector due to the breaking of the cylindrical symmetry. We first consider the field distribution in the plane of the dipole [Fig. 4(a)]. The emission with the $k$ vector parallel to the dipole has a plasmonic character. Similar to the case of the $z$ dipole, this emission is entirely lost in a planar HMM. However, in the patterned case, the cylinder corner promotes scattering of this emission into free space. The emission has a predominantly photonic character. In the planar HMM case, some of this emission misses the collection angle and is therefore lost. However, in the case of the patterned HMM [Fig. 4(b)], some of these losses are mitigated by scattering at the exterior edge of the groove at $r = r_g$). Thus, the nano-groove patterning helps to direct the emission with different $k$ vectors into the collection angle. The collection efficiency for the $r$ dipole is higher than 35% over the entire wavelength range and reaches almost 70% at 685 nm [Fig. 2(b)]. The dip at 725 nm [Fig. 2(b)] is caused by a resonant coupling of the emission to the exterior planar HMM.

Dipolar emitters coupled to hyperbolic metamaterials constitute a viable approach to fast and efficient photon sources. Tailored patterning of an HMM surface significantly enhances the photon collection efficiency with a high potential for room-temperature applications. To achieve efficient collection of radiation, we propose a design with a single nano-groove, which can be implemented using standard nanofabrication techniques. Depending on the dipole orientation and emission $k$ vector, different features of the proposed design are at play to promote efficient collection. Overall, the proposed structure promises a significantly higher collection efficiency over a broad emission spectrum (600–800 nm) for both dipole orientations compared to the case of a planar, unstructured HMM. At least a 16-fold increase in objective coupling efficiency over the

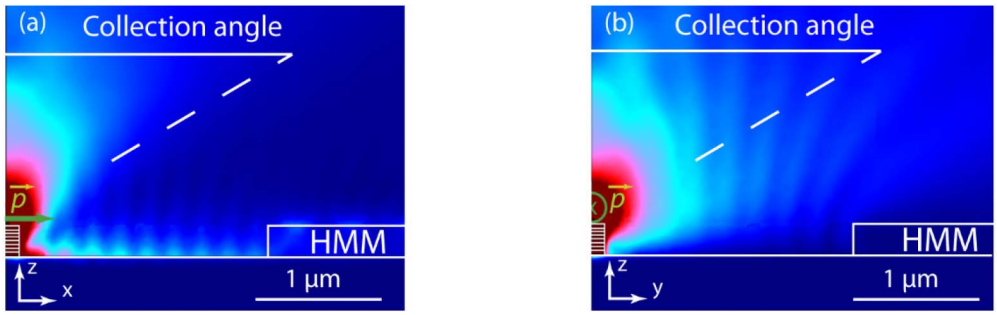


**Fig. 4.** Power density distribution for (a) in-plane and (b) out-of-plane $r$ dipole (green arrows) with a 685-nm emission wavelength placed on top of an HMM with a 2-μm groove. The exterior edge of the groove reflects back (a) the SPP and (b) photonic waves, resulting in extra contribution to $\beta$.

600–800 nm wavelength range is achieved for the $z$ dipole, and at least 35% efficiency is achieved for the $r$ dipole.

Our results can be experimentally validated using room-temperature NV centers in nanodiamonds and other types of solid-state quantum emitters. While we have previously demonstrated that random surface defects in planar HMMs could enhance outcoupling of SPP excited by NV centers [38], the proposed design offers a controllable approach to plasmon outcoupling. This approach promises an improved collection efficiency with a relatively moderate fabrication effort.

**Funding.** National Science Foundation (NSF) (DMR-1120923); Air Force Office of Scientific Research (AFOSR) (FA9550–12–1–0024, FA9550-14-1-0389).

**Acknowledgment.** The authors thank Alexey Akimov, Vadim Vorobyov, Stepan Bolshedvorskii, Vladimir Soshenko, and Vadim Kovalyuk for fruitful discussions and Deesha Shah for help with the paper preparation.

## REFERENCES

1. P. Kok, W. J. Munro, K. Nemoto, T. C. Ralph, J. P. Dowling, and G. J. Milburn, Rev. Mod. Phys. **79**, 135 (2007).
2. M. Leifgen, T. Schröder, F. Gädeke, R. Riemann, V. Métillon, E. Neu, C. Hepp, C. Arend, C. Becher, K. Lauritsen, and O. Benson, New J. Phys. **16**, 23021 (2014).
3. H. J. Kimble, Nature **453**, 1023 (2008).
4. R. Albrecht, A. Bommer, C. Deutsch, J. Reichel, and C. Becher, Phys. Rev. Lett. **110**, 243602 (2013).
5. T. Schröder, F. Gädeke, M. J. Banholzer, and O. Benson, New J. Phys. **13**, 55017 (2011).
6. E. Neu, D. Steinmetz, J. Riedrich-Möller, S. Gsell, M. Fischer, M. Schreck, and C. Becher, New J. Phys. **13**, 25012 (2011).
7. A. Sipahigil, K. D. Jahnke, L. J. Rogers, T. Teraji, J. Isoya, A. S. Zibrov, F. Jelezko, and M. D. Lukin, Phys. Rev. Lett. **113**, 113602 (2014).
8. I. Aharonovich, D. Englund, and M. Toth, Nat. Photonics **10**, 631 (2016).
9. J. Claudon, J. Bleuse, N. S. Malik, M. Bazin, P. Jaffrennou, N. Gregersen, C. Sauvan, P. Lalanne, and J.-M. Gérard, Nat. Photonics **4**, 174 (2010).
10. A. L. Falk, B. B. Buckley, G. Calusine, W. F. Koehl, V. V. Dobrovitski, A. Politi, C. A. Zorman, P. X.-L. Feng, and D. D. Awschalom, Nat. Commun. **4**, 1819 (2013).
11. A. J. Morfa, B. C. Gibson, M. Karg, T. J. Karle, A. D. Greentree, P. Mulvaney, and S. Tomljenovic-Hanic, Nano Lett. **12**, 949 (2012).
12. Y.-M. He, G. Clark, J. R. Schaibley, Y. He, M. Chen, Y. Wei, X. Ding, Q. Zhang, W. Yao, X. Xu, C. Lu, and J. Pan, Nat. Nanotechnol. **10**, 497 (2015).
13. J. M. Taylor, P. Cappellaro, L. Childress, L. Jiang, D. Budker, P. R. Hemmer, A. Yacoby, R. Walsworth, and M. D. Lukin, Nat. Phys. **4**, 810 (2008).
14. A. Laraoui, J. S. Hodges, and C. A. Meriles, Nano Lett. **12**, 3477 (2012).
15. L. Rondin, J. Tetienne, T. Hingant, J. Roch, P. Maletinsky, and V. Jacques, Rep. Prog. Phys. **77**, 56503 (2014).
16. K. V. Sreekanth, Y. Alapan, M. ElKabbash, E. Ilker, M. Hinczewski, U. A. Gurkan, A. De Luca, and G. Strangi, Nat. Mater. **15**, 621 (2016).
17. E. Bermúdez-Ureña, C. Gonzalez-Ballestero, M. Geiselmann, R. Marty, I. P. Radko, T. Holmgaard, Y. Alaverdyan, E. Moreno, F. J. García-Vidal, S. I. Bozhevolnyi, and R. Quidant, Nat. Commun. **6**, 7883 (2015).
18. J. T. Choy, I. Bulu, B. J. M. Hausmann, E. Janitz, I. Huang, and M. Lončar, Appl. Phys. Lett. **103**, 161101 (2013).
19. J. Riedrich-Möller, L. Kipfstuhl, C. Hepp, E. Neu, C. Pauly, F. Mücklich, A. Baur, M. Wandt, S. Wolff, M. Fischer, S. Gsell, M. Schreck, and C. Becher, Nat. Nanotechnol. **7**, 69 (2012).
20. D. Englund, B. Shields, K. Rivoire, F. Hatami, J. Vučković, H. Park, and M. D. Lukin, Nano Lett. **10**, 3922 (2010).
21. G. M. Akselrod, C. Argyropoulos, T. B. Hoang, C. Ciracì, C. Fang, J. Huang, D. R. Smith, and M. H. Mikkelsen, Nat. Photonics **8**, 835 (2014).
22. A. G. Curto, G. Volpe, T. H. Taminiau, M. P. Kreuzer, R. Quidant, and N. F. van Hulst, Science **329**, 930 (2010).
23. C. Belacel, B. Habert, F. Bigourdan, F. Marquier, J.-P. Hugonin, S. Michaelis de Vasconcellos, X. Lafosse, L. Coolen, C. Schwob, C. Javaux, B. Dubertret, J.-J. Greffet, P. Senellart, and A. Maitre, Nano Lett. **13**, 1516 (2013).
24. A. Mohtashami, T. Coenen, A. Antoncecchi, A. Polman, and A. F. Koenderink, ACS Photon. **1**, 1134 (2014).
25. R. Filter, J. Qi, C. Rockstuhl, and F. Lederer, Phys. Rev. B **85**, 125429 (2012).
26. H. A. Abudayyeh and R. Rapaport, Quantum Sci. Technol. **2**, 34004 (2017).
27. T. Galfsky, H. N. S. Krishnamoorthy, W. Newman, E. E. Narimanov, Z. Jacob, and V. M. Menon, Optica **2**, 62 (2015).
28. A. F. Koenderink, ACS Photon. **4**, 710 (2017).
29. D. R. Smith and D. Schurig, Phys. Rev. Lett. **90**, 77405 (2003).
30. L. Ferrari, C. Wu, D. Lepage, X. Zhang, and Z. Liu, Prog. Quantum Electron. **40**, 1 (2015).
31. Z. Jacob, L. V. Alekseyev, and E. Narimanov, Opt. Express **14**, 8247 (2006).
32. H. N. S. Krishnamoorthy, Z. Jacob, E. Narimanov, I. Kretzschmar, and V. M. Menon, Science **336**, 205 (2012).
33. C. L. Cortes, W. Newman, S. Molesky, and Z. Jacob, J. Opt. **16**, 129501 (2014).
34. V. V. Klimov, A. A. Pavlov, D. V. Guzatov, I. V. Zabkov, and V. D. Savinov, Phys. Rev. A **93**, 33831 (2016).
35. X. Ni, G. V. Naik, A. V. Kildishev, Y. Barnakov, A. Boltasseva, and V. M. Shalaev, Appl. Phys. B **103**, 553 (2011).
36. M. A. Noginov, H. Li, Y. A. Barnakov, D. Dryden, G. Nataraj, G. Zhu, C. E. Bonner, M. Mayy, Z. Jacob, and E. E. Narimanov, Opt. Lett. **35**, 1863 (2010).
37. J. Kim, V. P. Drachev, Z. Jacob, G. V. Naik, A. Boltasseva, E. E. Narimanov, and V. M. Shalaev, Opt. Express **20**, 8100 (2012).
38. M. Y. Shalaginov, V. V. Vorobyov, J. Liu, M. Ferrera, A. V. Akimov, A. Lagutchev, A. N. Smolyaninov, V. V. Klimov, J. Irudayaraj, A. V. Kildishev, A. Boltasseva, and V. M. Shalaev, Laser Photon. Rev. **9**, 120 (2015).
39. W. D. Newman, C. L. Cortes, and Z. Jacob, J. Opt. Soc. Am. B **30**, 766 (2013).
40. L. Ferrari, D. Lu, D. Lepage, and Z. Liu, Opt. Express **22**, 4301 (2014).
41. V. P. Drachev, V. A. Podolskiy, and A. V. Kildishev, Opt. Express **21**, 15048 (2013).
42. A. Poddubny, I. Iorsh, P. Belov, and Y. Kivshar, Nat. Photonics **7**, 948 (2013).
43. T. Galfsky, Z. Sun, C. R. Considine, C. Chou, W. Ko, Y. Lee, E. E. Narimanov, and V. M. Menon, Nano Lett. **16**, 4940 (2016).
44. D. Lu, J. J. Kan, E. E. Fullerton, and Z. Liu, Nat. Nanotechnol. **9**, 48 (2014).
45. C. Guclu, T. S. Luk, G. T. Wang, and F. Capolino, Appl. Phys. Lett. **105**, 123101 (2014).
46. P. R. West, S. Ishii, G. V. Naik, N. K. Emani, V. M. Shalaev, and A. Boltasseva, Laser Photon. Rev. **4**, 795 (2010).
47. B. Saha, S. Saber, G. V. Naik, A. Boltasseva, E. A. Stach, E. P. Kvam, and T. D. Sands, Phys. Status Solidi **252**, 251 (2015).
48. P. B. Johnson and R. W. Christy, Phys. Rev. B **6**, 4370 (1972).
49. V. E. Babicheva, M. Y. Shalaginov, S. Ishii, A. Boltasseva, and A. V. Kildishev, Opt. Express **23**, 31109 (2015).